

# Mini-Mesh: Practical Assessment of a Miniaturized IEEE 802.11n/s Mesh Testbed

Michael Rethfeldt, Benjamin Beichler, Hannes Raddatz, Felix Uster,  
Peter Danielis, Christian Haubelt, Dirk Timmermann

Institute of Applied Microelectronics and Computer Engineering, University of Rostock, Germany  
firstname.lastname@uni-rostock.de

**Abstract**—WLAN mesh networks are one of the key technologies for upcoming smart city applications and characterized by a flexible and low-cost deployment. The amendment IEEE 802.11s introduces low-level mesh interoperability at the WLAN MAC layer. On the physical layer, IEEE 802.11n introduced major improvements such as HT data rates, MIMO techniques, and frame aggregation. However, building large-scale 802.11n/s testbeds and reproducible setups is challenging and costly. On the other hand, existing attempts for down-scaling real-world setups are limited to works without support for 802.11n and 802.11s. We therefore present Mini-Mesh, a miniaturized indoor 802.11n/s testbed. Following a transmission range scaling approach, we deploy a 6x6-node mesh grid on an area of only  $1 m^2$ . We validate the applicability of our method via comparative measurements, exhibiting a deviation of less than 6 % between a scaled indoor and unscaled outdoor setup. Based on these results, we parameterize a path loss model helping us to estimate outdoor dimensions for arbitrary indoor mesh topologies.

## I. INTRODUCTION

Since 2011, the IEEE 802.11s (.11s) amendment standard enables low-level interoperability, integrating mesh mechanisms directly into the WLAN MAC layer [1]. As a promising core technology for future wireless communication networks, .11s is subject to ongoing research that aims at optimizing the interplay with existing network applications and protocols. On the physical layer, IEEE 802.11n (.11n) introduced major improvements such as HT data rates, MIMO techniques, and frame aggregation, pursued by IEEE 802.11ac and upcoming amendments. We aim at investigating own optimization strategies for .11s mesh networks, running on top of a .11n physical layer. However, the setup of large-scale .11n/s testbeds is costly and often impracticable. On the other hand, existing attempts for down-scaling real-world setups are limited to works without support for .11n and .11s.

Consequently, we present *Mini-Mesh*, a miniaturized indoor 802.11n/s testbed. Following a transmission range scaling approach, we deploy a 6x6-node mesh grid on an area of only  $1 m^2$ . We validate the applicability of our method via comparative measurements, exhibiting a deviation of less than 6 % between a scaled indoor and unscaled outdoor setup. As second major contribution, we parameterize a path loss model based on our practical results, helping us to estimate outdoor dimensions for arbitrary indoor mesh topologies.

## II. TECHNOLOGICAL BASICS

### A. IEEE 802.11n MIMO WLAN

The original IEEE 802.11 (.11) standard [1] was published in 1997 and describes the implementation of data communication in a Wireless Local Area Network (WLAN) in the 2.4 GHz ISM band and with a data rate of up to 2 Mbps. In 1999, the amendments 802.11a (.11a) and 802.11b (.11b) were ratified. Besides other changes, .11b enabled an increased data rate of 11 Mbps, still in the 2.4 GHz band, whereas .11a utilized the

5 GHz band and introduced Orthogonal Frequency-Division Multiplexing (OFDM) to support data rates of up to 54 Mbps. In 2003, the 802.11g amendment adopted the core functionality of .11a into the 2.4 GHz band.

802.11n (.11n) was published in 2009. It supports both the 2.4 GHz and 5 GHz band and defines an extended rate set with new modulation and coding schemes (MCS). MIMO functionality is introduced to use multiple transmit and receive antennas (up to 4 each). Different techniques like sender-side Space-Time Block Coding (STBC) and receiver-side Maximum Ratio Combining (MRC) are provided for diversity MIMO, employing the effect of multi-path propagation to improve SNR. Other .11n features include a doubled 40 MHz channel width and the support of spatial multiplexing (SM), a parallel transmission of independent data streams over multiple antennas for physical-layer data rates of up to 600 Mbps. Besides the physical-layer extensions, another important improvement is the use of MAC-layer frame aggregation and block acknowledgments.

The most recent amendment 802.11ac (.11ac) describes the logical evolution of .11n regarding more complex MCS schemes and MIMO technologies. However, it moves out of scope since practical combination of .11ac and .11s has just recently been made possible for selected Atheros chipsets under Linux and driver support is still under heavy development.

### B. IEEE 802.11s Mesh WLAN

As the first common industry WLAN mesh standard, the amendment .11s was ratified in September 2011 [1]. It enables vendor-independent infrastructure-less multi-hop communication based on the widespread .11 technology. Mesh functions like peering and routing are directly integrated into the MAC layer. To ensure interoperability, every .11s node must support the Hybrid Wireless Mesh Protocol (HWMP) and Airtime Link Metric (ALM) for mesh routing [2]. Mesh paths are chosen according to the ALM. It estimates the time cost for frame transmissions, considering protocol overhead, data rate, and error probability. The Linux WLAN MAC layer (kernel module *mac80211*) contains the currently most sophisticated implementation of .11s [3].

## III. RELATED WORK

The surveys [4]–[7] provide an overview of .11 research fields and existing real-world testbeds. However, no .11s setups are discussed yet and only few testbeds with a scaling approach are included. In Table I, we briefly summarize these and further works in the mesh testbed domain that are related to our approach. All works are grouped based on the .11 variants, the kind of scaling methods (if any), and the setup environment (indoor/outdoor). Additionally, the testbed size span (in #nodes) is given for each group. As a first category, we consider real-world setups that support both .11n and .11s. Some of them only implement preliminary .11s or allow no joint operation with

TABLE I: Comparison of Related Work  
(ID: Indoor, OD: Outdoor, AA: Attenuated Antennas, AC: Attenuated Cables, TP: Transmit Power, \*: preliminary .11s)

Works	.11 Variants	Mesh Routing	# Nodes	Scaling Method	Environment
Lin et al. [8], Imboden et al. [9]	n + s*	static / N/A	6–9	—	ID
Chakraborty et al. [10], Sajjadi et al. [11], Krug et al. [12], Makris et al. [13]	n + s	HWMP	2–120	—	ID / OD
Pojda et al. [14], Hayat et al. [15]	n + s	HWMP	3–6	TP	ID / OD
EWANT [16], MiNT [17], Bonsai [18], Meraka [19], IvyNet [20], ScaleMesh [21], Bialkowski et al. [22], FloorNet [23], Intel Research, Seoul National University [5]	a / b / g	AODV, OLSR, DYMO, DSR, LOF, HSLS	3–210	AA / AC / TP	ID
MeshTest [24], ORBIT [4], WHYNET / Castadiva / MNE [6]	a / b / g	AODV, OLSR	10–64	AA / AC / TP	ID / OD
Mini-Mesh	a/n + s	HWMP	36	AA + TP	ID / OD

.11n [8], [9]. Apart from [14] and [15], using a reduced transmit power for multi-hop measurements between UAV nodes, no scaling methods are discussed. As a second category, we list earlier works dealing with testbed miniaturization. However, they are limited to .11a/b/g and do neither support .11n nor .11s.

In contrast to the related work, our approach *Mini-Mesh* presents a miniaturized mesh testbed for the joint analysis of .11n and .11s. We use both signal attenuators and power reduction for down-scaling the transmission range in a line-of-sight (LoS) indoor setup. As a tool for estimating the corresponding outdoor dimensions to prospective indoor topologies, we interpret an existing propagation model and parameterize it through comparative measurements.

#### IV. MINI-MESH: TESTBED PREPARATION

In this section, we introduce our miniaturized .11n/s testbed *Mini-Mesh*. The main objectives of our approach are:

- Real-world testbed with support for .11n & .11s
- Extensible small-scale indoor lab deployment
- Applicability to large-scale outdoor scenarios
- High reproducibility of experiments
- Low-cost HW platform with versatile NIC support
- Highly configurable SW platform (OS and drivers)

After describing the general setup, we identify platform-specific performance limitations to assess the practical operating points for our scaling method.

##### A. General Setup and Target Geometry

Our testbed comprises 36 Intel Galileo single-board computers [26]. In contrast to commercial .11 AP hardware, these devices run a full-featured Linux while still offering an mPCIe interface. This was necessary to equip the nodes with .11 NIC from the Atheros product family, supported by the *ath9k* driver. It is the currently most configurable and versatile .11 driver but recent hardware is mostly limited to mPCIe cards.

TABLE II: Testbed Configuration

Parameter	Value
Device	Intel Galileo Board (Gen. 1)
CPU	Quark X1000 (Single-Core 400 MHz)
RAM	256 MB DDR3
OS	Debian 8 (Linux Kernel v4.9)
.11 NIC	Compex WLE200NX .11a/b/g/n (mPCIe)
NIC Chipset	Atheros AR9280 ( <i>ath9k</i> driver)
Antennas	2 x 5 dBi Dual-Band Omni-Direct.
Antenna Cables	2 x 20 cm U.FL-RP-SMA
Attenuators	2 x Mini-Circuits VAT-30+ (30 dB)
Channel	149 (5745 MHz, HT20, Long GI)

Table II shows the hardware and software configuration of the devices. All nodes run a Debian 8 OS with mainline Linux kernel v4.9, integrating the .11(s) software MAC layer. Each node is equipped with a .11n capable Atheros NIC. It supports operating in diversity and spatial multiplexing MIMO modes, using two RX and TX chains and up to two spatial streams. Two omni-directional dual-band antennas (5 dBi gain, 6 cm inter-antenna distance) are attached to the NIC by means of 20 cm pigtail cables. For indoor scaling purposes, we interpose fixed 30 dB RF attenuators at each antenna connector [27].

To prevent external interference on the testbed as much as possible, all devices operate on the practically unused 5 GHz channel 149. While channels 149–165 are considered for regular .11a operation in North America and other countries, European regulations permit their use only with maximum TX power of 25 mW. Hence, for a fine-grained range control within the regulatory and technical limits of our testbed, TX power is configurable in 1 dBm steps between 0 (1 mW) and 14 dBm (25 mW) per TX chain. This results in a minimum of 3 dBm (2 mW) and a maximum of 17 dBm (50 mW) for the dual-antenna configuration.

Table III shows the NIC capabilities concerning maximum TX power and RX sensitivity for all supported .11n MCS. We further consider the effective power limits on channel 149. Theoretical physical-layer rates are given, assuming 20 MHz HT mode with long guard interval (GI). Note that most .11 consumer hardware and drivers, including our *ath9k* based NIC, do not support “greenfield” operation with .11n-only rates. Instead, a “mixed mode” is used where .11n HT rates only apply for unicast data frames whereas other frame types (management/control/action and multicast) are transmitted at legacy .11a rates. Therefore, corresponding .11a rates and NIC properties are given as well. However, there is no legacy rate match for MCS 7/15 (marked in red).

To enable investigation of arbitrary multi-hop scenarios, the nodes are arranged in a 6x6-node regular grid setup. Requiring an approximate indoor area of 1 m<sup>2</sup> only, this allows for a testbed extension to more than 100 nodes in our lab environment. Fig. 1 shows a magnified extract of the current testbed geometry. As result of the dual-antenna configuration, adjacent nodes are placed at a distance of 20 cm in horizontal, 26 cm in vertical, and 33 cm in diagonal direction. By limiting the communication range to 33 cm <d< 40 cm, direct data transmission is possible only between physical grid neighbors. This is achieved by applying fixed RF attenuators and TX power reduction, as explained in Section V. Multi-hop paths between non-neighboring nodes are automatically formed on-demand by the .11s mesh routing protocol HWMP.

##### B. Platform Performance Analysis

In order to assess the performance limitations of our testbed and select suitable operating points, we measured the maximum

TABLE III: .11n MCS Rate Table and WLE200NX Transceiver Capabilities (Max. TX Pwr. (per TX Chain; 14 dBm Restriction on Chan. 149) and RX Sensitivity according to [25])

.11n Properties (5GHz, HT20, Long GI)							.11a Properties		
MCS	# Spat. Streams	Mod.	FEC	Rate [Mbps]	Max. TX Pwr. [dBm]	RX Sens. [dBm]	Rate [Mbps]	Max. TX Pwr. [dBm]	RX Sens. [dBm]
0	1	BPSK	1/2	6.5	17 (14)	-93	6	17 (14)	-94
1	1	QPSK	1/2	13	17 (14)	-91	12	17 (14)	-93
2	1	QPSK	3/4	19.5	17 (14)	-87	18	17 (14)	-90
3	1	16-QAM	1/2	26	17 (14)	-85	24	17 (14)	-86
4	1	16-QAM	3/4	39	17 (14)	-82	36	15 (14)	-83
5	1	64-QAM	2/3	52	16 (14)	-77	48	13	-79
6	1	64-QAM	3/4	58.5	12	-75	54	12	-75
7	1	64-QAM	5/6	65	8	-72	54	12	-75
8	2	BPSK	1/2	13	17 (14)	-93	6	17 (14)	-94
9	2	QPSK	1/2	26	17 (14)	-91	12	17 (14)	-93
10	2	QPSK	3/4	39	17 (14)	-87	18	17 (14)	-90
11	2	16-QAM	1/2	52	17 (14)	-85	24	17 (14)	-86
12	2	16-QAM	3/4	78	17 (14)	-82	36	15 (14)	-83
13	2	64-QAM	2/3	104	16 (14)	-77	48	13	-79
14	2	64-QAM	3/4	117	12	-75	54	12	-75
15	2	64-QAM	5/6	130	8	-72	54	12	-75

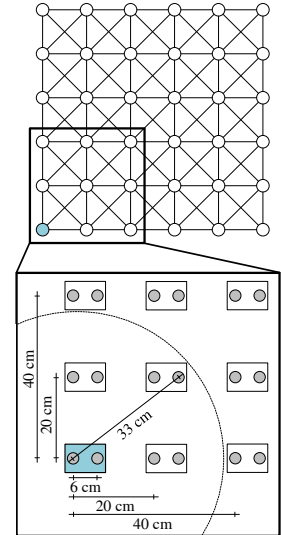


Fig. 1: 6x6 Dual-Antenna Mesh Grid Geometry

TCP/UDP throughput achievable at each .11n rate (MCS) supported by the NIC. De facto optimal channel conditions were created by placing two nodes 30 cm apart, configured at maximum  $P_{tx}$  of 17 dBm and without RF attenuators. We used default Linux kernel and iperf TCP settings, including 1448 bytes MSS and CUBIC congestion control. However, we deactivated the CUBIC “HyStart” mechanism that inhibited TCP window growth, confirmed as a problem for recent kernel versions [28]. Regarding UDP, we used 1448 bytes datagrams and a 1 MB socket buffer size. We averaged 5 measurement runs for each configuration of data rate and transport protocol. Duration of each run was 60 s with throughput samples taken in 1 s intervals, leading to a total of 300 samples per configuration. Performance data were obtained from the iperf application.

Table IV shows sender- and receiver-side perceived TCP/UDP throughput, packet loss (UDP), and CPU utilization (iperf process) for each MCS configuration. At MCS 0–3 (one data stream, diversity MIMO) and 8–9 (two streams, spatial multiplexing), marked in green, expectable TCP and UDP net throughput is achieved with CPU loads of less than 60%. At higher MCS rates, marked in red, receiver- or sender-side performance limits are reached. Note that for MCS 4 and 10, the sender is still able to transmit at the target rate. However, high CPU utilization and packet loss in the UDP results reveal a receiver-side performance limit. In case of TCP, sender-side congestion control can still mitigate the problem. To exclude general .11 NIC and network stack limitations as a possible problem cause, we conducted measurements at MCS 15 using more powerful PC hardware (Dell Latitude E4300). We achieved close to 100 Mbps UDP net throughput at CPU loads below 15%. Additionally, we repeated TCP/UDP measurements using two Galileo boards connected via Fast Ethernet. Thereby, we mainly replaced MAC-layer and driver code path, I/O interface, and NIC. Showing decent Ethernet throughput, we assume Galileo platform-specific issues related to the interplay of Linux WLAN stack, *ath9k* driver, and .11 NIC. We plan a detailed investigation as future work. Summarized, MCS 3 and 9 currently represent the highest stable single- and dual-stream rates achievable, before hitting performance limits of our testbed devices. In what follows, MCS 0–3 and 8–9 are considered as suitable operating points.

## V. MINI-MESH: TRANSMISSION RANGE SCALING APPROACH

For down-scaling the maximum transmission range in our testbed, we build on the fundamentals of the “ScaleMesh” approach [21]. Its authors present a miniaturized .11a/b/g testbed in which they apply variable RF attenuators but otherwise use only one fixed data rate and transmit power. As in [21], our approach applies attenuators at each antenna connector. However, instead of relying on costly variable attenuators, we only consider cheap fixed attenuators for our 36 dual-antenna nodes. Attenuation substantially reduces the achievable transmission range by multiple orders of magnitude, to lab dimensions of only a few meters. We experimentally determined an attenuation level of 30 dB per antenna that allows us to perform remaining fine-tuning via transmit power variation for all .11n data rates configurable in our testbed (see Section IV-B). Given our grid geometry in Fig. 1, aiming at

TABLE IV: Max. Link Throughput and CPU Load Comparison (GB: Galileo Board; TP: Throughput; SND: Sender; RCV: Receiver; \*: Test with two PC nodes; ETH: Test with Fast Ethernet (GB))

MCS (GB)	TCP			UDP			
	TP [Mbps]	SND CPU [%]	RCV CPU [%]	TP [Mbps]	Loss [%]	SND CPU [%]	RCV CPU [%]
0	4.7	2.5	9.7	5.8	0	7.8	9.7
1	9.2	4.9	22.5	11.5	0	15.1	18.4
2	13.4	7.6	25.5	17.2	0	22.5	28.0
3	17.8	11.2	46.7	22.9	0	29.6	38.2
4	26.7	20.5	57.1	26.5	23	37.5	89.5
5	16.7	98.2	43.1	23.5	0	98.6	57.4
6	16.6	98.1	43.6	23.4	0	98.5	56.9
7	16.6	98.2	43.6	23.3	0	98.4	56.2
8	9.1	4.9	20.0	11.5	0	12.9	25.6
9	17.4	10.8	42.1	22.9	0	26.4	56.5
10	26.8	20.8	54.9	26.9	22	37.7	88.9
11	16.9	98.1	45.5	23.5	0	98.4	57.6
12	16.9	98.0	44.2	23.3	0	98.3	55.5
13	17.3	98.1	44.6	23.1	0	98.2	54.5
14	17.0	98.4	45.3	23.1	0	98.3	54.3
15	16.9	98.5	44.8	22.5	0	98.5	57.4
15 *	71.5	1.3	7.5	96.8	0	11.5	13.0
ETH	94.1	11.2	49.0	96.1	0	30.9	32.8

1-hop-only neighborhoods, we adjust the transmit power for each data rate until we obtain an indoor range between 33 and 40 cm.

To derive a simplified mathematical description of our method, we follow the power and path loss model considerations described by the authors in [21]. As opposed to them, we do not prescribe a given propagation environment and do not aim at calculating variable attenuation levels for different indoor scaling points. Instead, we measure the indoor and outdoor transmission range achieved with and without fixed attenuators for each data rate, using the indoor power levels needed for our grid geometry. Afterwards, we obtain the propagation model coefficient that serves as a conversion factor between lab setup and outdoor environment. It will help us to draw conclusions about corresponding outdoor dimensions also for future miniaturized indoor topologies. In the following, we briefly state the theoretical basis of our approach. We denote a miniaturized indoor range as “scaled” (S). The corresponding outdoor range will be denoted as “unscaled” (U).

The *Equivalent Isotropic Radiated Power* (EIRP) of a sending node can be expressed as  $EIRP = P_{tx} + G_{ant}$ . Here,  $P_{tx}$  denotes the transmit power, fine-tuned for the desired indoor range, and  $G_{ant}$  the antenna gain (connector cable attenuation neglected). For an aligned and equally polarized dual-antenna system,  $P_{tx}$  is the sum of both transmit chains (+3 dBm) [29]. Overall signal attenuation  $\Omega_{tot}$  between a sending and receiving node is given in Eq. 1 as a general function of power levels as well as a function of distance-dependent path loss  $\Omega_{PL}(d)$ , antenna gains  $G_{ant}$ , and optional RF attenuators for both unscaled and scaled scenario.

$$\begin{aligned}\Omega_{tot} &= P_{tx} - P_{rx} \\ \Omega_{tot}^U &= \Omega_{PL}(d) - 2 \cdot G_{ant} \\ \Omega_{tot}^S &= \Omega_{PL}(d) - 2 \cdot G_{ant} + 2 \cdot \Omega_{att}\end{aligned}\quad (1)$$

In the case of scaling,  $\Omega_{att}$  expresses the fixed RF attenuators at the sender- and receiver-side antennas (30 dB each).  $P_{rx}$  denotes the signal power level received at node  $R$ , observed after antenna gain and potential RF attenuators. Note that for each .11n data rate (Modulation and Coding Scheme – MCS) the respective RX sensitivity threshold for successful data reception represents the lower limit for  $P_{rx}$  (see Table III). Since an increase in modulation order leads to a decrease in energy per bit, a higher SNR is needed to successfully decode the signal [29]. This limits the maximum transmission range for a specific rate configuration. Summarized, the only difference between scaled and unscaled transmission range in our approach lies in the application of RF attenuators. Therefore,  $G_{ant}$  and  $P_{tx}$  are equal in both cases. Likewise,  $P_{rx}$  takes the same value for the corresponding scaled and unscaled operating points at maximum stable transmission range. Note that we consider a simplified transmission path scenario with dominating Line-of-Sight (LoS) component. Thus, we assume the SNR improvement of transmit/receive diversity MIMO, comprised in  $P_{rx}$ , to be equal in both cases as well.

$$\Omega_{PL}(d) = 20 \cdot \log_{10}(f_c) + 10 \cdot p \cdot \log_{10}(d) \quad (2)$$

According to the ITU-R propagation model [21], path loss between a sender/receiver pair can be expressed as a function of distance  $d$ , frequency  $f_c$ , and a path loss coefficient  $p$  (see Eq. 2). Thereby, the choice of  $p$  depends on the propagation environment and ranges from 2 (free space) to 5 (dense indoor scenarios). Authors in [21] assume  $p=3$  (“office area”) when using the ITU model to calculate different indoor scaling points.

$$\begin{aligned}\Omega_{PL}(d^U) &= P_{tx} - P_{rx} + 2 \cdot G_{ant} \\ \Omega_{PL}(d^S) &= P_{tx} - P_{rx} + 2 \cdot G_{ant} - 2 \cdot \Omega_{att}\end{aligned}\quad (3)$$

Combining the expressions of Eq. 1 and Eq. 2, as given in Eq. 3, we can derive unscaled and scaled distance, resulting into Eq. 4. After substitution, we can write the outdoor/indoor scaling ratio  $r$  as shown in Eq. 5.

$$\begin{aligned}\log_{10}(d^U) &= \frac{P_{tx} - P_{rx} + 2 \cdot G_{ant} - 20 \cdot \log_{10}(f_c)}{10 \cdot p} \\ \log_{10}(d^S) &= \frac{P_{tx} - P_{rx} + 2 \cdot G_{ant} - 2 \cdot \Omega_{att} - 20 \cdot \log_{10}(f_c)}{10 \cdot p} \\ r = \frac{d^U}{d^S} &= 10^{\frac{2 \cdot \Omega_{att}}{10 \cdot p}} \rightarrow p = \frac{2 \cdot \Omega_{att}}{10 \cdot \log_{10}(r)}\end{aligned}\quad (4)$$

$$r = \frac{d^U}{d^S} = 10^{\frac{2 \cdot \Omega_{att}}{10 \cdot p}} \rightarrow p = \frac{2 \cdot \Omega_{att}}{10 \cdot \log_{10}(r)} \quad (5)$$

Having measured the distance pairs  $[d^S, d^U]$  experimentally for each rate/power configuration [MCS,  $P_{tx}$ ], we will be able to calculate coefficient  $p$  according to Eq. 5. Using this simplified model, for any transmission range configured in the scaled indoor testbed by variation of  $P_{tx}$ , the equivalent unscaled outdoor distance (without attenuators) can be estimated using Eq. 4. Thereby,  $p$  represents the model parameter for conversion between arbitrary indoor and outdoor LoS scenarios.

## VI. MINI-MESH: SCALING IMPLEMENTATION

We practically applied our scaling approach and experimentally determined the path loss factor  $p$  of Eq. 5 that allows for a conversion between indoor and outdoor setup dimensions. Therefore, we conducted comparative range measurements with a pair of testbed devices configured as given in Table II. Unless noted otherwise, we use default Linux network stack and driver parameters. Starting with indoor measurements in our lab, we applied 30 dB RF attenuators at each antenna. Experiments were run for the .11n subset MCS0–3 and 8–9, due to the performance limitations of our testbed (see Section IV-B). As stated in Section IV-A, devices operate in a “mixed mode” of .11n data frame and .11a basic/multicast frame rates. Hence, .11n/a rate combinations were configured as given in Table III.

Due to space constraints, we do not elaborate on a number of different practical issues we identified and counteracted before achieving reproducible distance results. Briefly summarized, it was necessary to wrap all node housings in adhesive copper tape to ensure a proper RF shielding. We further deactivated certain chipset-specific mechanisms via *ath9k* driver options, including *Ambient Noise Immunity* (ANI) and periodic noise floor calibration.

At each configuration, we determined  $P_{tx}$  required for a certain maximum stable link management distance  $d_{L_{max}}$  (beacons, link handshake) and HT data frame transmission distance  $d_{D_{max}}$ . We varied  $P_{tx}$  (3 to 17 dBm dual-antenna sum) until reaching a stable indoor transmission range of  $33 \text{ cm} < d_{D_{max}} < 40 \text{ cm}$ , needed for the desired 1-hop-only neighborhood in our testbed (see Fig. 1). In all measurements, the devices faced one another like vertical neighbors in the grid setup. As  $d_{L_{max}}$ , we denote the distance where  $P_{rx}$  just reaches the NIC’s sensitivity threshold for the configured .11a rate. Here, mesh links were still being continuously refreshed every second by beacons, received from the opposite peer. Contrary, at  $d_{D_{max}}$ ,  $P_{rx}$  just reaches the sensitivity threshold for the configured .11n rate. Here, ping packets (data frames) of size 1400 bytes, sent in 1 s intervals, were still transmitted successfully with one-digit millisecond RTT, not yet showing outliers or timeouts. Hence, in mixed mode a stable link, maintained via .11a management frames, does not inherently guarantee stable .11n data frame transmission and thus  $d_{D_{max}} \leq d_{L_{max}}$ . Measures were taken with centimeter accuracy

TABLE V: Indoor/Outdoor Range, Scaling Ratio  $r$ , and Coeff.  $p$  for MCS 0–3 (1SS) & 8–9 (2SS) (SS: Spatial Streams;  $\Omega_{att}$ : Attenuation,  $P_{tx}$ : TX Power,  $d_L$ : Link Range,  $d_D$ : Data Frame Range)

.11n MCS	.11a Rate [Mbps]	$P_{tx}$ [dBm]	ID ( $2 \cdot \Omega_{att}$ : 60 dB)		OD ( $2 \cdot \Omega_{att}$ : 0 dB)		OD/ID Ratio $r$		Coeff. $p$	
			$d_{L_{max}}$ [m]	$d_{D_{max}}$ [m]	$d_{L_{max}}$ [m]	$d_{D_{max}}$ [m]	$d_L$	$d_D$	$d_L$	$d_D$
0	6	7	0.40	0.38	224	210	560	553	2.18	2.19
1	12	9	0.40	0.38	223	202	558	532	2.18	2.20
2	18	11	0.38	0.36	216	212	568	589	2.18	2.17
3	24	14	0.39	0.36	213	210	546	583	2.19	2.17
8	6	13	0.72	0.38	412	23	572	61	2.18	3.37
9	12	15	0.74	0.38	410	23	554	61	2.19	3.37
							$\varnothing r_{1SS}$ : 562	$\varnothing p_{1SS}$ : 2.18		
							$\varnothing r_{2SS}$ : 61	$\varnothing p_{2SS}$ : 3.37		

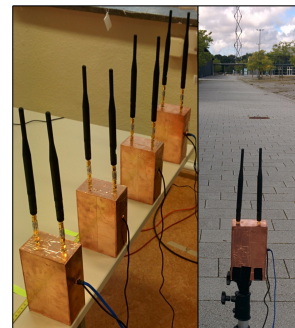


Fig. 2: ID/OD Measurements

at the highest possible distance where the respective behavior could be observed throughout multiple minutes. Subsequent to the indoor experiments, everything was repeated with meter accuracy in an outdoor setting. The same device pair was now mounted on tripods 1 m above ground, keeping the indoor rate/power configurations but not using attenuators. Measurements were conducted on the fairground boulevard at the IGA Park premises in Rostock, Germany, providing a maximum line-of-sight of more than 400 meters (see right part of Fig. 2).

Table V shows the indoor and outdoor results. For each MCS rate the associated TX power  $P_{tx}$  is given, experimentally determined for the target indoor data frame transmission range  $33 \text{ cm} < d_{D_{max}} < 40 \text{ cm}$ . As expected for the operation in .11a/n mixed mode, link range  $d_{L_{max}}$  is always higher than  $d_{D_{max}}$ . Since action and management frames for peering and link maintenance are sent at .11a legacy rates, they exhibit lower SNR requirements than the .11n MCS rates used for data frames. For MCS 0–3, applying diversity MIMO (one spatial stream (1SS)) to all frame types, this amounts to only a small difference between  $d_{D_{max}}$  and  $d_{L_{max}}$  in our LoS scenario. Contrary, MCS 8 and 9 transmit data frames with 2SS spatial multiplexing MIMO, whereas the corresponding legacy rate frames are transmitted in diversity mode. Hence, these operating points reveal a considerable difference between  $d_{L_{max}}$  and  $d_{D_{max}}$ . This observation confirms previous simulation studies, indicating comparable range results for SISO and diversity MIMO but inferior performance of spatial multiplexing in LoS scenarios due to the minor influence of multi-path propagation [30].

Comparing the outdoor and indoor results, the qualitative range characteristics still persist without attenuators. For 1SS diversity MIMO we determined outdoor ranges of 200–225 m (MCS 0–3 link and data frame range; 36–40 cm indoors) and 410–412 m (MCS 8/9 link range only; 72–74 cm indoors), resulting in a mean outdoor-to-indoor scaling ratio  $r$  of approx. 560. For these configurations, following Eq. 5, we derive path loss coefficient  $p \approx 2.18$  as suitable model parameter. Comparing ITU reference values for  $p$ , this would closely correspond to a free-space environment ( $p=2$ ) [21]. Single-stream results for  $r$  and  $p$  are highlighted in green in Table V. Regarding 2SS spatial multiplexing (MCS 8/9 data frames), the LoS drawbacks are amplified outdoors due to the complete absence of reflecting walls and ceilings. In our lab environment, the desired data frame range of 36–38 cm could be achieved both in 1SS and 2SS mode for the given configurations of  $P_{tx}$ . While measuring an equal outdoor  $d_{D_{max}}$  of 23 m at MCS 8 and 9, confirming the correct choice of  $P_{tx}$ , it lies an order of magnitude below the corresponding 1SS outdoor results. Without considerable expansion of our model, we account for the different multi-path propagation characteristics

by summarizing the effects into path loss coefficient  $p$ . Hence, we obtain a scaling ratio  $r \approx 60$  and coefficient  $p \approx 3.37$  for the 2SS mode, still lying within ITU parameter range [21]. Our dual-stream results are highlighted in blue in Table V. Summarized, having derived the model parameters for 1SS and 2SS rate configuration, we obtain a mathematical description to convert between indoor and outdoor LoS setups.

## VII. EXPERIMENTAL VALIDATION

To demonstrate the applicability of our approach, we conducted comparative indoor and outdoor throughput measurements. Using up to four devices and iperf v3.2, we determined TCP and UDP end-to-end throughput for a single link as well as a 2- and 3-hop chain topology. Note that we achieved a maximum data frame transmission range  $d_{D_{max}}$  of more than 200 m outdoors. To enable 3-hop positioning within a 450 m distance along the IGA Park premises, we defined a hop distance of  $0.6 \cdot d_{D_{max}}$  for all throughput measurements (indoor and outdoor). This way, multi-hop forwarding was ensured without nodes being skipped. Remaining device parameters and scaling points were kept as described in the previous section. We further used the same TCP/UDP settings as in our initial performance analysis (Section IV-B). Beginning indoors, we noticed a considerable performance breakdown during the multi-hop measurements, especially for UDP. We identified the hidden terminal problem as root cause and could mitigate it by activating the optional request/clear-to-send (RTS/CTS) mechanism. We then used it by default in the outdoor measurements. This observation contradicts earlier works that evaluated RTS/CTS in .11a/b/g networks [21], but confirms investigations that recommend its use in .11n networks with frame aggregation. There, the expenses of losing aggregated frames outweigh the handshaking overhead of RTS/CTS [31].

As in our performance analysis (Section IV-B), we averaged 300 throughput samples for each configuration of path length, transport protocol, data rate, and RTS/CTS. We observed the same qualitative characteristics between indoor and outdoor scenario at all rate configurations. Therefore and due to space constraints, only results for MCS 3 are presented. Fig. 3 compares the results of the scaled (S) indoor and unscaled (U) outdoor setup. To illustrate the hidden terminal effects, indoor results are shown for RTS/CTS both turned off and on. Outdoor results are given for RTS/CTS activated only. Following the indoor results, TCP takes benefit from RTS/CTS already over 1 hop (5% improvement). Due to its bidirectional nature, TCP exhibits a higher collision probability compared to UDP in this case. Over 2 and especially 3 hops, TCP congestion control helps to moderate the hidden terminal problem to some extent, even without prior handshaking. Still, using RTS/CTS improves TCP throughput by

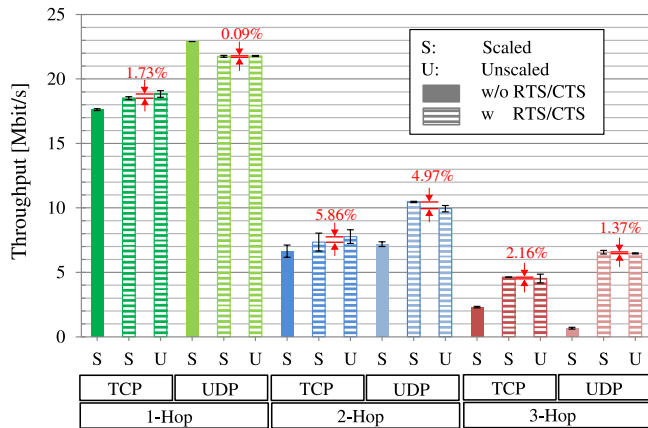


Fig. 3: Scaled vs. Unscaled TCP/UDP Throughput

9% in the 2-hop and 50% in the 3-hop case. Regarding UDP, RTS/CTS comes as overhead in the 1-hop case but considerably improves performance over multiple hops (31% over 2 hops, 90% over 3 hops). Since there is no reliability or congestion control mechanism, UDP suffers from increased collisions and the lack of sender-side rate throttling. Comparing outdoor and indoor measurements, average variation is below 6%, with a slightly higher standard deviation in TCP results (below 2%). This validates the applicability of results, obtained in our scaled testbed, to prospective outdoor setups that can be estimated using the parameterized model described in Sections V and VI.

## VIII. CONCLUSION

We present *Mini-Mesh*, a miniaturized testbed for the joint evaluation of 802.11n/s mesh networks. Employing a transmission range scaling approach, we deploy a 6x6-node grid topology on an area of only  $1 m^2$ , in contrast to  $\sim(545 \times 545) m^2$  without scaling measures (MCS3 rate configuration). In a city scenario, this would correspond to a large public place or facility, such as a University campus. We validate the applicability of our method via comparative measurements, exhibiting a deviation of less than 6% between a scaled indoor and unscaled outdoor setup. Based on these results, we parameterize a simple path loss model helping us to estimate outdoor dimensions for arbitrary indoor mesh topologies in single- and dual-stream MIMO configuration. In future research, we will use our full testbed to evaluate application and protocol behavior and prototype cross-layer optimization approaches in different mesh network scenarios.

## IX. ACKNOWLEDGMENTS

We would like to thank the German Federal Institute for Research on Building, Urban Affairs and Spatial Development (BBSR) within the Federal Office for Building and Regional Planning for their support in this project.

## REFERENCES

- [1] "IEEE Standard for Information Technology - Telecommunications and Information Exchange between Systems - Local and Metropolitan Area Networks - Specific Requirements Part 11: Wireless LAN Medium Access Control (MAC) and Physical Layer (PHY) Specifications," *IEEE Std 802.11-2012 (Revision of IEEE Std 802.11-2007)*, 2012.
- [2] S. Bari, F. Anwar, and M. Masud, "Performance study of hybrid wireless mesh protocol (HWMP) for IEEE 802.11s WLAN mesh networks," in *2012 ICCCE*. IEEE, 2012, pp. 712–716.
- [3] open80211s, 2017. [Online]. Available: <http://www.o11s.org/>
- [4] B. Blywis, M. Guenes, F. Juraschek, and J. H. Schiller, "Trends, advances, and challenges in testbed-based wireless mesh network research," *Mobile Networks and Applications*, vol. 15, no. 3, p. 315, Jun. 2010.

- [5] S. Uludag, T. Imboden, and K. Akkaya, "A taxonomy and evaluation for developing 802.11-based wireless mesh network testbeds," *International Journal of Communication Systems*, vol. 25, no. 8, pp. 963–990, 2012.
- [6] K. N. Patel *et al.*, "A survey on emulation testbeds for mobile ad-hoc networks," *Procedia Computer Science*, vol. 45, pp. 581–591, 2015.
- [7] P. Serrano, P. Salvador, V. Mancuso, and Y. Grunenberger, "Experimenting with commodity 802.11 hardware: overview and future directions," *IEEE Communications Surveys & Tutorials*, vol. 17, no. 2, pp. 671–699, 2015.
- [8] Y.-D. Lin, S.-L. Chang, J.-H. Yeh, and S.-Y. Cheng, "Indoor deployment of IEEE 802.11s mesh networks: Lessons and guidelines," *Ad Hoc Networks*, vol. 9, no. 8, pp. 1404–1413, 2011.
- [9] T. Imboden, K. Akkaya, and Z. Moore, "Performance evaluation of wireless mesh networks using IEEE 802.11s and IEEE 802.11n," in *2012 IEEE ICC*. IEEE, 2012, pp. 5675–5679.
- [10] S. Chakraborty and S. Nandi, "Controlling unfairness due to physical layer capture and channel bonding in 802.11 n+s wireless mesh networks," in *Proceedings of the 2015 International Conference on Distributed Computing and Networking*. ACM, 2015, p. 21.
- [11] D. Sajjadi, M. Tanha, and J. Pan, "A comparative study of channel switching latency for conventional and SDN-based routing in multi-hop multi-radio Wireless Mesh Networks," in *2016 13th IEEE CCNC*. IEEE, 2016, pp. 330–334.
- [12] S. Krug, A. Brychcy, and J. Seitz, "A mobile embedded-Linux-based testbed for outdoor ad hoc network evaluation," in *2016 IEEE WiSEE*. IEEE, 2016, pp. 164–166.
- [13] N. Makris, T. Korakis, V. Maglogiannis, D. Naudts, N. Nikaein *et al.*, "Flex testbed: a platform for 4g/5g wireless networking research." ICT Fire Book November 2016, 2016, pp. 1–25.
- [14] J. Pojda, A. Wolff, M. Sbeiti, and C. Wietfeld, "Performance analysis of mesh routing protocols for UAV swarming applications," in *2011 8th ISWCS*. IEEE, 2011, pp. 317–321.
- [15] S. Hayat, E. Yanmaz, and C. Bettstetter, "Experimental analysis of multipoint-to-point UAV communications with IEEE 802.11n and 802.11ac," in *2015 26th IEEE PIMRC*. IEEE, 2015, pp. 1991–1996.
- [16] S. Sanghani, T. X. Brown, S. Bhandare, and S. Doshi, "EWANT: The emulated wireless ad hoc network testbed," in *2003 IEEE WCNC*, vol. 3. IEEE, 2003, pp. 1844–1849.
- [17] P. De, A. Raniwala, S. Sharma, and T.-c. Chiueh, "MiNT: A miniaturized network testbed for mobile wireless research," in *2005 24th IEEE INFOCOM*, vol. 4. IEEE, 2005, pp. 2731–2742.
- [18] V. Naik, E. Ertin, H. Zhang, and A. Arora, "Wireless Testbed Bonsai," in *2006 4th IEEE WiOpt*. IEEE, 2006, pp. 1–9.
- [19] A. A. Lysko and D. L. Johnson, "A study of propagation effects in a wireless test bed," *WSEAS Transactions on Communications*, vol. 7, no. 8, pp. 857–871, 2008.
- [20] Y. Su and T. Gross, "Validation of a miniaturized wireless network testbed," in *2008 3rd ACM WiNTECH*. ACM, 2008, pp. 25–32.
- [21] S. M. ElRakabawy, S. Frohn, and C. Lindemann, "A scalable dual-radio wireless testbed for emulating mesh networks," *Wireless Networks*, vol. 16, no. 8, pp. 2191–2207, 2010.
- [22] K. Bialkowski and M. Portmann, "Design of testbed for wireless mesh networks," in *2010 IEEE APSURSI*. IEEE, 2010, pp. 1–4.
- [23] P. Serrano, C. J. Bernardos, A. de La Oliva, A. Banchs, I. Soto, and M. Zink, "Floornet: deployment and evaluation of a multi-hop wireless 802.11 testbed," *EURASIP Journal on Wireless Communications and Networking*, vol. 2010, p. 8, 2010.
- [24] T. C. Clancy and B. D. Walker, "MeshTest: Laboratory-based wireless testbed for large topologies," in *2007 3rd TridentCom*. IEEE, 2007, pp. 1–6.
- [25] Compex, "WLE200NX," 2017. [Online]. Available: <http://www.compex.com.sg/product/wle200nx/>
- [26] Intel Galileo Gen1, 2017. [Online]. Available: <http://ark.intel.com/products/78919/Intel-Galileo-Board>
- [27] Mini-Circuits, "VAT-30+ Signal Attenuators," 2017. [Online]. Available: <http://www.minicircuits.com/pdfs/VAT-30.pdf>
- [28] GT Mailing List, "TCP reaching to maximum throughput after a long time," 2017. [Online]. Available: <https://lists.gt.net/linux/kernel/2414672>
- [29] J. Geier, *Designing and deploying 802.11n wireless networks*. Pearson Education, 2010.
- [30] M. Rethfeldt, H. Raddatz, B. Beichler, B. Konieczek, D. Timmermann, C. Haubelt, and P. Danielis, "ViPMesh: A Virtual Prototyping Framework for IEEE 802.11s Wireless Mesh Networks," in *2016 IEEE WiMob*. IEEE, 2016, pp. 1–7.
- [31] Y.-D. Lin, J.-H. Yeh, T.-H. Yang, C.-Y. Ku, S.-L. Tsao, and Y.-C. Lai, "Efficient dynamic frame aggregation in IEEE 802.11s mesh networks," *International Journal of Communication Systems*, vol. 22, no. 10, pp. 1319–1338, 2009.